Hindawi Publishing Corporation
Indian Journal of Materials Science
Volume 2013, Article ID 356025, 6 pages
http://dx.doi.org/10.1155/2013/356025

Research Article

Enhanced Photocatalytic Degradation of Methylene Blue Using $ZnFe_2O_4$/MWCNT Composite Synthesized by Hydrothermal Method

Sonal Singhal,[1] Rimi Sharma,[1] Charanjit Singh,[1] and S. Bansal[2]

[1] *Department of Chemistry, Panjab University, Chandigarh 160 014, India*
[2] *Department of Science and Technology, New Delhi, India*

Correspondence should be addressed to Sonal Singhal; sonal1174@gmail.com

Received 3 July 2013; Accepted 31 July 2013

Academic Editors: W. Cantwell, D. Das, and W. Gurnule

Multiwalled carbon nanotubes (MWCNTs) were synthesized using arc discharge method at a magnetic field of 430 G and purified using HNO_3/H_2O_2. Transmission electron micrographs revealed that MWCNTs had inner and outer diameter of ~2 nm and ~4 nm, respectively. Raman spectroscopy confirmed formation of MWCNTs showing G-band at 1577 cm^{-1}. $ZnFe_2O_4$ and $ZnFe_2O_4$/MWCNT were produced using one step hydrothermal method. Powder X-ray diffraction (XRD) confirmed the formation of cubic spinel $ZnFe_2O_4$ as well as incorporation of MWCNT into $ZnFe_2O_4$. Visible light photocatalytic degradation of methylene blue (MB) was studied using pure $ZnFe_2O_4$ and $ZnFe_2O_4$/MWCNT. The results showed that $ZnFe_2O_4$/MWCNT composite had higher photocatalytic activity as compared to pure $ZnFe_2O_4$. After irradiation for 5 hours in the visible light, MB was almost 84% degraded in the presence of $ZnFe_2O_4$ photocatalyst, while 99% degradation was observed in case of $ZnFe_2O_4$/MWCNT composite. This enhancement in the photocatalytic activity of composite may be attributed to the inhibition of recombination of photogenerated charge carriers.

1. Introduction

Solar energy active photocatalysts have been a promising material for an environmental purification process. Efforts have been made to synthesize materials capable of utilizing solar spectrum for the photo degradation of industrial waste pollutants and dyes [1]. A wide use of dyes as redox indicators, biological stains, and pharmaceutical industries had adverse effects on gastrointestinal, genitourinary, and cardiovascular system of human body [2, 3]. Degradation of organic pollutants and dyes such as methylene blue, bromophenol blue, and Chicago sky blue from industrial waste water remains as a challenge because of low visible light photo catalytic activity of metal oxides and sulphides [4–6]. Large band gap of ZnS, TiO_2, $SrTiO_3$, and Ag_3VO_4 [7–9] prevents their functioning as effective catalyst for visible light photo degradation [10].

However, the advantage of ferrites as photo catalysts is their capability to absorb visible light solar irradiation because of low band gap and large availability of catalytic sites for adsorption of noxious waste and dyes [11]. Also, ferrites are magnetic [12–15] in nature giving them added advantage of easy recovery after photocatalytic reaction.

Albeit, the numerous literature has been reported on the photo degradation of different dyes using $ZnFe_2O_4$ as catalyst having spinel structure, where Zn^{2+} cations occupy tetrahedral site and Fe^{3+} enters octahedral site [16]. The band gap of $ZnFe_2O_4$ is small (1.9 eV) due to which it utilizes visible light to act as a photocatalyst [17]. Fan et al. [18] prepared nanocrystalline $ZnFe_2O_4$ by hydrothermal method and investigated photodegradation of acid orange II azo dye. The authors observed better photocatalytic activity as compared to bulk $ZnFe_2O_4$ sample prepared by conventional solid state method. The effect of sintering temperature on photodegradation of methyl orange was studied by Jadhav et al. [11] and observed maximum activity for samples sintered at 500°C. Su et al. [19] synthesized $ZnFe_2O_4$ by hydrothermal

process and reported photodegradation of acid orange II dye within 2 hours. Li et al. [20] synthesized spinel zinc ferrite nanospheres of 212 nm and noticed enhanced photo catalytic activity of the $ZnFe_2O_4$ nanospheres as compared to $ZnFe_2O_4$ nanoparticles in the decomposition of rhodamine B. However, low quantum efficacy as a photo catalyst of the zinc ferrite has been improved by loading $ZnFe_2O_4$ to titanium dioxide [10]. Main drawback of $ZnFe_2O_4/TiO_2$ composite is that it can absorb only UV light in predominance and only 50% of the dye degrades.

Therefore, the process of photo degradation requires absorption of visible light form solar or artificial sources. For the purpose of improving photo catalytic activity of the ferrites and to efficiently utilize visible light, a high aspect ratio and tubular nanometric dimensions of multiwalled carbon nanotubes (MWCNTs) make themselves a prospective candidate for photo catalytic activity [21, 22]. Decoration of CNTs surface by foreign materials especially metal oxides [23] extends their field of application and improves their chemical, electrical, mechanical, and thermal properties that can be used in advanced nanotechnology [24]. Magnetic CNT composites have been found to be a potential alternate in future for materials with low photo catalytic activity. Degradation of organic pollutants and toxic dyes has been an important aspect to study the photo catalytic efficiency of magnetic CNT composites [25].

Thus, our effort is to synthesize MWCNTs by arc discharge method. This method is advantageous over other previously reported methods because it is a low cost method which gives completely aligned multiwalled carbon nanotubes of high purity. Further, the surface of MWCNTs was decorated by $ZnFe_2O_4$. This was envisaged so as to efficiently design a green nanocomposite for the absorption of visible light from the spectrum. One step hydrothermal process is employed to produce $ZnFe_2O_4$ and $ZnFe_2O_4$/MWCNTs composite. Combination of two semiconductors, that is, $ZnFe_2O_4$ and MWCNT, would enhance the photo catalytic activity. Due to enhancement in photochemical activity of $ZnFe_2O_4$/MWCNTs composite, it is found to degrade almost 99% of the MB dye.

2. Experimental

2.1. Synthesis of MWCNTs. A metal-free arc discharge method was used to synthesize MWCNTs. An arc excitation between the graphite rods submerged in the deionized water was carried out by applying an AC voltage of 50 V to generate 100 A of current. The schematic diagram for the same is given in Figure 1. The electromagnets having soft iron core and copper wire winding around the core serve the purpose for the generation of 430 Gauss of magnetic field in a direction perpendicular to the arcing rods. The gap between the inter electrodes was maintained at a separation of ~0.5 mm for the generation of arc. A gap control screw unit was used for the movement of graphite electrodes. Carbon soot was produced by discharging graphite electrodes for 1 hr, and liquid turned black which was separated by decantation. This product formed was washed with de-ionized water 3-4 times followed by refluxing with 8 M aqueous HNO_3 for 24 hrs. The sample was then refluxed again in 30% H_2O_2 as done by Feng et al. [26] for 24 hrs for further removal of impurities left. pH was then neutralized by washing the sample with de-ionized water. The sample was air dried and annealed at 400°C for 30 minutes.

2.2. Synthesis of $ZnFe_2O_4$/MWCNT Nanocomposite. A variety of methods are available to synthesize ferrites [27–31], but here $ZnFe_2O_4$ and $ZnFe_2O_4$/MWCNT were prepared by hydrothermal process [32]. The starting materials, that is, ferric nitrate, zinc nitrate, and sodium hydroxide, used for the preparation were of analytical grade. 10 mmol of ferric nitrate and 5 mmol of zinc nitrate were dissolved in minimum amount of water. 10 mg of prepared MWCNT was added into the solution and sonicated for 10 minutes. The pH of the solution was set to 12-13 with the help of 6 M sodium hydroxide. The mixture was vigorously stirred for 30 minutes and transferred into Teflon-lined stainless steel autoclave. The autoclave was sealed and maintained at 180°C for 12 hours. The product was allowed to cool to room temperature, filtered, and washed with distilled water followed by drying in vacuum oven for 12 hours. The same procedure was applied without adding MWCNT to get pure $ZnFe_2O_4$.

2.3. Photocatalytic Activity. The photocatalytic activity of $ZnFe_2O_4$ and $ZnFe_2O_4$/MWCNT was evaluated by degradation of aqueous solution of methylene blue (MB) under visible light irradiation. 50 mg of catalyst was added to 50 mL of 10 mg/L aqueous solution of MB. Before illumination, the mixture was stirred in dark for 30 min to achieve adsorption desorption equilibrium between catalyst and dye solution. The solution was exposed to visible light under stirring after addition of 2 mL of 30% H_2O_2. At given time intervals, 3 mL of aliquots was withdrawn and centrifuged to remove catalyst. The concentration of methylene blue in aqueous solution was determined with the help of UV-Vis spectrophotometer.

2.4. Physical Measurements. Transmission electron micrographs (TEM) were recorded using Hitachi (H7500) Transmission Electron microscope, operated at 120 kV. Raman data were recorded using Invia Raman Microscope (Renishaw) at room temperature with argon ion laser excitation 514 nm (5 mW power) over a range of 0–3200 cm^{-1}. X-ray diffractographs of the prepared samples were recorded using an X-ray diffractometer (model PANalytical's X'pert PRO spectrophotometer) with Cu-Kα radiation. Photoirradiation was carried out using 160 W Hg lamp. The concentration of methylene blue during the degradation was monitored by UV-visible spectrophotometer JASCO, V-530.

3. Results and Discussions

3.1. TEM Characterization. The morphology of the MWCNTs was studied using TEM analysis. The sample was agitated ultrasonically in ethanol for 20 minutes to avoid aggregation

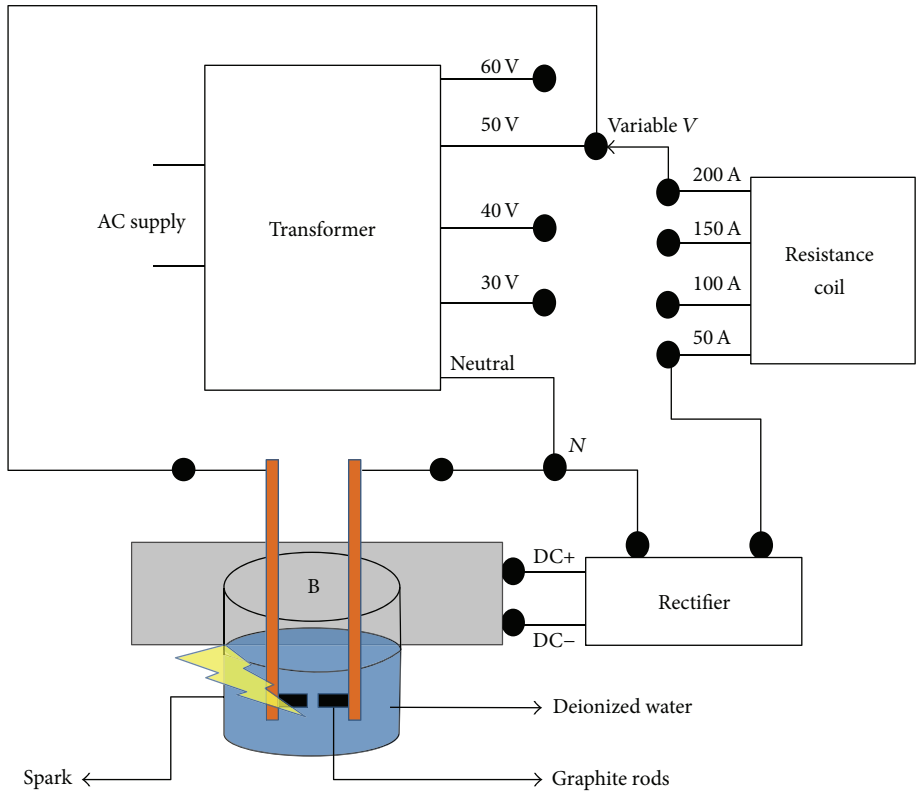

FIGURE 1: Schematic diagram of the arc discharge apparatus.

of the sample. Nanotubes thus obtained had inner and outer diameter of ~2 nm and ~4 nm. The corresponding wall thickness of ~2 nm can be attributed to the formation of approximately seven walled CNTs (interlayer distances between graphene sheets being 0.33 nm). The TEM micrographs of MWCNTs, after refluxing using HNO_3/H_2O_2 are shown in Figure 3 which indicated the formation of pure nanotubes. CNTs obtained after purification has cleaner surface without any amorphous carbon impurities. TEM image also revealed that there is no effect on the shape and surface morphology of MWCNTs. Hence, the obtained nanotubes were further used for the formation of nanocomposite.

3.2. Raman Spectroscopy. Raman spectroscopy revealed invaluable insights into the purification of nanotubes. G-band (1577 cm^{-1}) corresponded to the confirmation of MWCNTs. Defect induced D-band (1355 cm^{-1}) was minimized after purifying CNTs with HNO_3/H_2O_2 for 24 hrs as shown in Figure 4. D-band arises due presence of sp^3 hybrid carbon, whereas G-band is due to existence sp^2 hybrid carbon as in the case of MWCNTs. Intensity of D-Band is smaller when 430 Gauss of magnetic field was generated perpendicular to arcing rods. Occurrence of G-Band at 1581 cm^{-1} also confirmed that semiconducting MWCNTs were produced [33]. Large intensity of G′-Band at ~2700 cm^{-1} indicated the reduction of amorphous carbon [34]. These results were also supported by transmission electron microscopy (TEM). Decrease in the intensity of D-Band and increase in the intensity of G′-Band clearly confirmed the removal of amorphous carbon impurities and carbon lamellas from the MWCNT sample.

3.3. X-Ray Diffraction Studies. The phase composition of all the synthesized samples was investigated using powder X-ray diffraction (XRD) technique. XRD pattern of $ZnFe_2O_4$/MWCNT nanocomposite, pure $ZnFe_2O_4$, and MWCNT is presented in Figure 2. A strong diffraction peak at $2\theta = 26^\circ$ can be indexed to (002) plane of MWCNT (Figure 2(a)) corresponding to the $P6_3/mmc$ space group. No peak corresponding to any other metal impurity was observed for purified sample. The lattice parameters were determined using the Powley and Le Bail refinement method, and the values of "a" and "c" were 2.45 Å and 6.75 Å , respectively, corresponding to the hexagonal structure of graphite [35]. The diffraction peaks of pure $ZnFe_2O_4$ (Figure 2(b)) confirmed formation of cubic spinel structure with Fd-3m space group. The peaks indexed to (220), (311), (400), (511), and (400) planes correspond to cubic spinel structure. The lattice parameter was calculated using the Powley refinement method and was found to be 8.46 Å. Based on the following

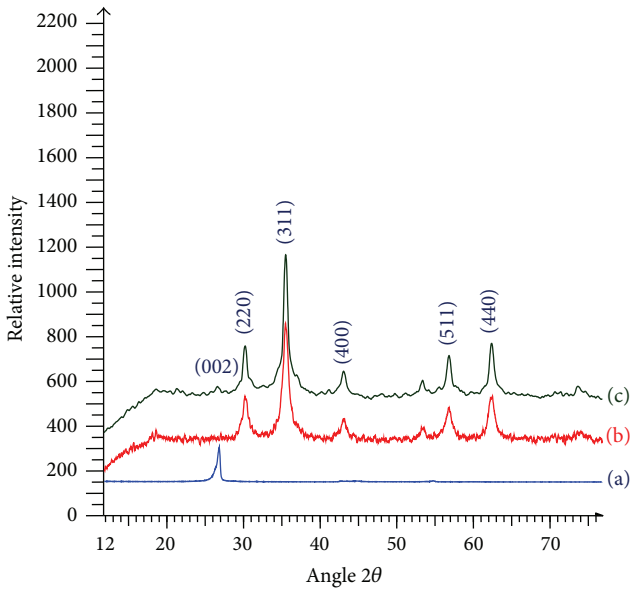

FIGURE 2: XRD patterns of (a) MWCNT, (b) $ZnFe_2O_4$, and (c) $ZnFe_2O_4$/MWCNT.

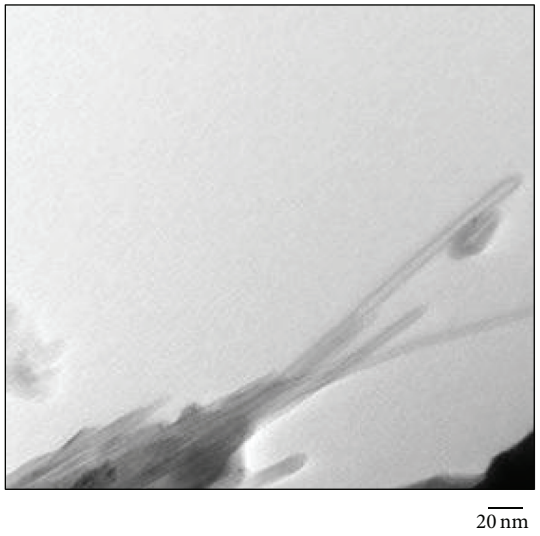

FIGURE 3: TEM image of MWCTs after purifying with HNO_3: 24 hrs/H_2O_2: 24 hrs.

Debye-Scherrer relation [36], crystallite size was found to be 10 nm.

$$d = \frac{0.9\lambda}{\beta \cos\theta}, \tag{1}$$

where d is the diameter of the particle, β is the full width of half maximum (FWHM), λ is the X-ray wavelength (1.542 Å), and θ is the angle of diffraction. In case of $ZnFe_2O_4$/MWCNT composite (Figure 2(c)), besides the diffraction peaks of $ZnFe_2O_4$, a new peak at $2\theta = 26^\circ$ was also observed indicating coexistence of $ZnFe_2O_4$ and MWCNT in the composite. However, the intensity of the peak is low due to addition of very small amount of MWCNT.

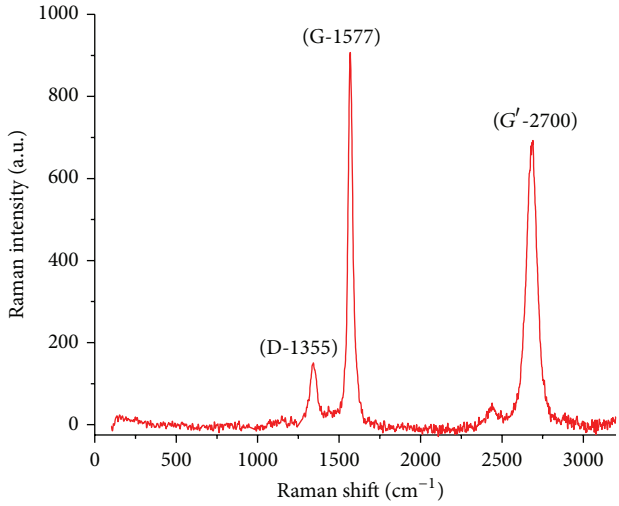

FIGURE 4: Raman spectra of MWCNTs obtained after purification with HNO_3: 24 hrs/H_2O_2: 24 hrs.

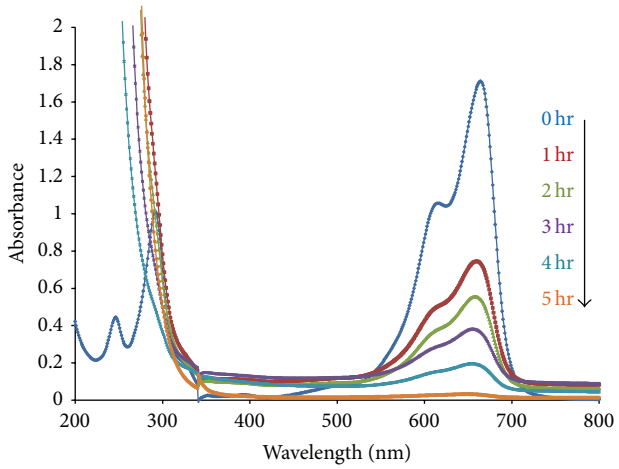

FIGURE 5: Change in absorption with time in the presence of $ZnFe_2O_4$/MWCNT.

3.4. Photocatalytic Activity. The photocatalytic activities of $ZnFe_2O_4$ and $ZnFe_2O_4$/MWCNT nanocomposite were evaluated by degradation of methylene blue (MB) solution. Figure 5 shows degradation of MB in the presence of $ZnFe_2O_4$/MWCNT nanocomposite under visible light irradiation. The UV-visible spectra of MB solution show four characteristic peaks at 246, 292, 617, and 663 nm. Addition of H_2O_2 masks peaks at 246 and 292 nm, while the peaks at 617 and 663 nm regularly decrease in intensity with increasing irradiation time. The peak at 664 nm disappeared completely in 5 hours indicating complete degradation (~99%) of MB dye. The photocatalytic degradation was calculated by applying following [37]:

$$\%\ \text{degradation} = \left(\frac{C_o - C_t}{C_o}\right) \times 100, \tag{2}$$

where C_o is initial MB concentration and C_t is the concentration of MB at time t. For comparison, the degradation

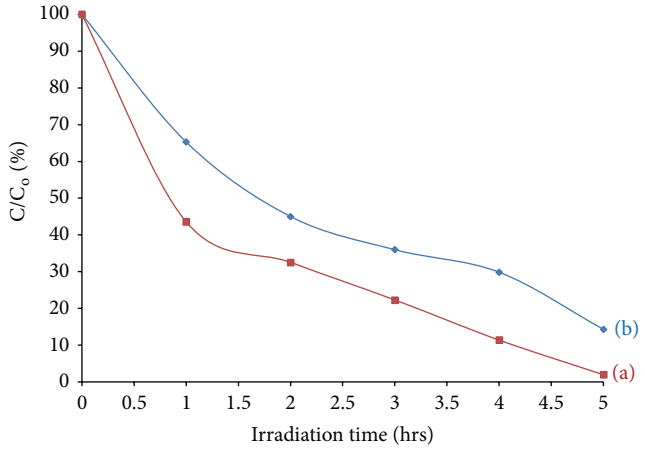

FIGURE 6: Effect of catalysts (a) $ZnFe_2O_4$/MWCNT and (b) $ZnFe_2O_4$ on decomposition of methylene blue.

of MB was performed using pure $ZnFe_2O_4$. Photocatalytic degradation efficiency of MB in the presence of $ZnFe_2O_4$ and $ZnFe_2O_4$/MWCNT nanocomposite is shown in Figure 6. It was observed that after irradiation for 5 hours, about 84% of MB was degraded in the presence of $ZnFe_2O_4$ photocatalyst, while 99% degradation was observed in case of composite. Therefore, it can be concluded that $ZnFe_2O_4$/MWCNT nanocomposite exhibits stronger photocatalytic activity as compared to pure ferrite. This may be due to stronger interaction between $ZnFe_2O_4$ and MWCNT which inhibited recombination of photogenerated charge carriers.

4. Conclusion

An economical arc discharge method was used to synthesize multiwalled carbon nanotubes. Predominance of MWCNTs having diameter of around 2–4 nm in the prepared sample was clearly shown by TEM image. Oxidizing agent HNO_3/H_2O_2 was used to purify the MWCNTs without affecting the surface of nanotubes. Raman spectra show the peak intensity of D- and G′-bands which clearly revealed the purity of as-synthesized carbon nanotubes. Decrease in the intensity of defect induced D-band at 1350 cm^{-1} and increase in the intensity of G′-band at 2700 cm^{-1} indicating the removal of amorphous carbon. Further synthesis of $ZnFe_2O_4$ and $ZnFe_2O_4$/MWCNT composite was successfully carried out using one step hydrothermal method. Formation of composite was confirmed using XRD. The peaks indexed to (220), (311), (400), (511), and (400) planes correspond to cubic spinel structure along with a very small peak of CNTs. A comparative photocatalytic study of $ZnFe_2O_4$ and $ZnFe_2O_4$/MWCNT nanocomposite clearly indicated the enhancement of photocatalytic activity in $ZnFe_2O_4$/MWCNT nanohybrid. MB was almost 84% degraded in the presence of $ZnFe_2O_4$ photocatalyst, while 99% degradation was observed in case of $ZnFe_2O_4$/MWCNT composite after irradiation for 5 hours in the visible light. MWCNTs significantly enhance photocatalytic activity of $ZnFe_2O_4$ as strong interaction between $ZnFe_2O_4$ and MWCNT inhibits recombination of photo generated carriers.

Acknowledgment

The authors are highly grateful to the Council of Scientific and Industrial Research (CSIR) for providing the necessary financial support.

References

[1] P. Xiong, Y. Fu, L. Wang, and X. Wang, "Multi-walled carbon nanotubes supported nickel ferrite: a magnetically recyclable photocatalyst with high photocatalytic activity on degradation of phenols," *Chemical Engineering Journal*, vol. 195-196, pp. 149–157, 2012.

[2] B. Mokhlesi, J. B. Leikin, P. Murray, and T. C. Corbridge, "Adult toxicology in critical care part II: specific poisonings," *Chest*, vol. 123, no. 3, pp. 897–922, 2003.

[3] J. W. Harvey and A. S. Keitt, "Studies of the efficacy and potential hazards of methylene blue therapy in aniline-induced methaemoglobinaemia," *British Journal of Haematol*, vol. 54, pp. 29–41, 1982.

[4] M. A. Gibson and J. W. Hightower, "Oxidative dehydrogenation of butenes over magnesium ferrite kinetic and mechanistic studies," *Journal of Catalysis*, vol. 41, no. 3, pp. 420–430, 1976.

[5] E. Manova, T. Tsoncheva, D. Paneva, I. Mitov, K. Tenchev, and L. Petrov, "Mechanochemically synthesized nano-dimensional iron-cobalt spinel oxides as catalysts for methanol decomposition," *Applied Catalysis A*, vol. 277, no. 1-2, pp. 119–127, 2004.

[6] P. Baldrian, V. Merhautová, J. Gabriel et al., "Decolorization of synthetic dyes by hydrogen peroxide with heterogeneous catalysis by mixed iron oxides," *Applied Catalysis B*, vol. 66, no. 3-4, pp. 258–264, 2006.

[7] S. Boumaza, A. Boudjemaa, A. Bouguelia, R. Bouarab, and M. Trari, "Visible light induced hydrogen evolution on new heterosystem $ZnFe_2O_4/SrTiO_3$," *Applied Energy*, vol. 87, no. 7, pp. 2230–2236, 2010.

[8] S. Xu, W. Shangguan, J. Yuan, J. Shi, and M. Chen, "Preparations and photocatalytic degradation of methyl orange in water on magnetically separable $Bi_{12}TiO_{20}$ supported on nickel ferrite," *Science and Technology of Advanced Materials*, vol. 8, no. 1-2, pp. 40–46, 2007.

[9] Y. Yang, Z. Cao, Y. Jiang, L. Liu, and Y. Sun, "Photoinduced structural transformation of $SrFeO_3$ and $Ca_2Fe_2O_5$ during photodegradation of methyl orange," *Materials Science and Engineering B*, vol. 132, no. 3, pp. 311–314, 2006.

[10] B. Zhang, J. Zhang, and F. Chen, "Preparation and characterization of magnetic $TiO_2/ZnFe_2O_4$ photocatalysts by a sol-gel method," *Research on Chemical Intermediates*, vol. 34, no. 4, pp. 375–380, 2008.

[11] S. D. Jadhav, P. P. Hankare, R. P. Patil, and R. Sasikala, "Effect of sintering on photocatalytic degradation of methyl orange using zinc ferrite," *Materials Letters*, vol. 65, no. 2, pp. 371–373, 2011.

[12] X. Liu and W. Gao, "Preparation and magnetic properties of $NiFe_2O_4$ nanoparticles by modified pechini method," *Materials and Manufacturing Processes*, vol. 27, no. 9, p. 905, 2012.

[13] M. Drofenik, M. Kristl, D. Makovec, Z. Jagličić, and D. Hanžel, "Preparation and study of zinc ferrite nanoparticles with a high magnetization," *Materials and Manufacturing Processes*, vol. 23, no. 6, pp. 603–606, 2008.

[14] H. Xu and H. Yang, "Magnetic properties of $Y_3Fe_5O_{12}$ nanoparticles doped Bi and Ce ions," *Materials and Manufacturing Processes*, vol. 23, no. 1, pp. 1–4, 2008.

[15] H. Y. He, "Synthesis and magnetic properties of $Co_{0.5}Zn_{0.5}Fe_2O_4$ nanoparticles by template-assisted combustion method," *Materials and Manufacturing Processes*, vol. 27, no. 9, p. 901, 2012.

[16] J. P. Singh, G. Dixit, R. C. Srivastava, H. M. Agrawal, V. R. Reddy, and A. Gupta, "Observation of bulk like magnetic ordering below the blocking temperature in nanosized zinc ferrite," *Journal of Magnetism and Magnetic Materials*, vol. 324, no. 16, pp. 2553–2559, 2012.

[17] X. Li, Y. Hou, Q. Zhao, W. Teng, X. Hu, and G. Chen, "Capability of novel $ZnFe_2O_4$ nanotube arrays for visible-light induced degradation of 4-chlorophenol," *Chemosphere*, vol. 82, no. 4, pp. 581–586, 2011.

[18] G. Fan, Z. Gu, L. Yang, and F. Li, "Nanocrystalline zinc ferrite photocatalysts formed using the colloid mill and hydrothermal technique," *Chemical Engineering Journal*, vol. 155, no. 1-2, pp. 534–541, 2009.

[19] M. Su, C. He, V. K. Sharmab et al., "Mesoporous zinc ferrite: synthesis, characterization, and photocatalytic activity with H_2O_2/visible light," *Journal of Hazardous Materials*, vol. 211-212, pp. 95–103, 2012.

[20] X. Li, Y. Hou, Q. Zhao, and L. Wang, "A general, one-step and template-free synthesis of sphere-like zinc ferrite nanostructures with enhanced photocatalytic activity for dye degradation," *Journal of Colloid and Interface Science*, vol. 358, no. 1, pp. 102–108, 2011.

[21] J. Salvetat, A. J. Kulik, J. Bonard et al., "Elastic modulus of ordered and disordered multiwalled carbon nanotubes," *Advanced Materials*, vol. 11, no. 2, pp. 161–165, 1999.

[22] W. Oh and M. Chen, "Synthesis and characterization of CNT/TiO_2 composites thermally derived from MWCNT and titanium(IV) n-butoxide," *Bulletin of the Korean Chemical Society*, vol. 29, no. 1, pp. 159–164, 2008.

[23] X. Wang, Z. Zhao, J. Qu, Z. Wang, and J. Qiu, "Fabrication and characterization of magnetic Fe_3O_4-CNT composites," *Journal of Physics and Chemistry of Solids*, vol. 71, no. 4, pp. 673–676, 2010.

[24] E. W. Wong, P. E. Sheehan, and C. M. Lieber, "Nanobeam mechanics: elasticity, strength, and toughness of nanorods and nanotubes," *Science*, vol. 277, no. 5334, pp. 1971–1975, 1997.

[25] W. Wang, P. Serp, P. Kalck, and J. L. Faria, "Visible light photodegradation of phenol on MWNT-TiO_2 composite catalysts prepared by a modified sol-gel method," *Journal of Molecular Catalysis A*, vol. 235, no. 1-2, pp. 194–199, 2005.

[26] Y. Feng, H. Zhang, Y. Hou et al., "Room temperature purification of few-walled carbon nanotubes with high yield," *ACS Nano*, vol. 2, no. 8, pp. 1634–1638, 2008.

[27] J. Chandradass, D. S. Bae, M. Balasubramanian, and K. H. Kim, "The influence of oleic acid to metal nitrate ratio on the particle size and magnetic properties of lanthanum ferrite nanoparticles by emulsion method," *Materials and Manufacturing Processes*, vol. 26, no. 2, pp. 230–235, 2011.

[28] L. J. Berchmans, V. Leena, K. Amalajyothi, S. Angappan, and A. Visuvasam, "Preparation of lanthanum ferrite substituted with MG and CA," *Materials and Manufacturing Processes*, vol. 24, no. 5, pp. 546–549, 2009.

[29] G. Chandrasekaran, "Spectroscopic study of autocombustion process in the synthesis of nano particles of Ni-Cu ferrite," *Materials and Manufacturing Processes*, vol. 22, no. 3, pp. 366–369, 2007.

[30] Y. H. Guu, K. Tsai, and L. Chen, "An experimental study on electrical discharge machining of manganese-zinc ferrite magnetic material," *Materials and Manufacturing Processes*, vol. 22, no. 1, pp. 66–70, 2007.

[31] H. Jiang, X. Wang, C. Yu, and L. Wang, "Molten salt synthesis of $Ni_{0.5}Zn_{0.5}Fe_2O_4$ powders," *Materials and Manufacturing Processes*, vol. 25, no. 12, pp. 1489–1493, 2010.

[32] N. Y. Mostafa, Z. I. Zaki, and Z. K. Heiba, "Structural and magnetic properties of cadmium substituted manganese ferrites prepared by hydrothermal route," *Journal of Magnetism and Magnetic Materials*, vol. 329, pp. 71–76, 2013.

[33] A. C. Ferrari, "Raman spectroscopy of graphene and graphite: disorder, electron-phonon coupling, doping and nonadiabatic effects," *Solid State Communications*, vol. 143, no. 1-2, pp. 47–57, 2007.

[34] J. Maultzsch, S. Reich, C. Thomsen et al., "Raman characterization of boron-doped multiwalled carbon nanotubes," *Applied Physics Letters*, vol. 81, no. 14, pp. 2647–2649, 2002.

[35] M. C. Schabel and J. L. Martins, "Energetics of interplanar binding in graphite," *Physical Review B*, vol. 46, no. 11, pp. 7185–7188, 1992.

[36] A. K. M. Akther Hossain and M. L. Rahman, "Enhancement of microstructure and initial permeability due to Cu substitution in $Ni_{0.50-x}CuxZn_{0.50}Fe_2O_4$ ferrites," *Journal of Magnetism and Magnetic Materials*, vol. 323, no. 15, pp. 1954–1962, 2011.

[37] M. M. Rashad, R. M. Mohamed, M. A. Ibrahim, L. F. M. Ismail, and E. A. Abdel-Aal, "Magnetic and catalytic properties of cubic copper ferrite nanopowders synthesized from secondary resources," *Advanced Powder Technology*, vol. 23, no. 3, pp. 315–323, 2012.